Increase of the superconducting T_c, irreversibility fields, and critical currents in tetragonal $YBaSrCu_{3-x}Mo_xO_{7+d}$

K. Rogacki
Physics Department, Northern Illinois University, DeKalb, Illinois 60115
and Institute of Low Temperature and Structure Research, Polish Academy of Sciences, 50-950 Wroclaw, Poland

B. Dabrowski and O. Chmaissem
Physics Department, Northern Illinois University, DeKalb, Illinois 60115

J. D. Jorgensen
Materials Science Division, Argonne National Laboratory, Argonne, Illinois 60439

(Received 8 July 1999; revised manuscript received 21 June 2000; published 22 December 2000)

Recently, we have investigated how the superconducting transition temperature T_c, critical currents j_c, and irreversibility fields B_{irr}, of compounds with multiple CuO_2 planes depend on physical properties and structural features of the blocking layer. To modify conductivity of the CuO chains in the blocking layer and decrease anisotropy of the $YBa_2Cu_3O_y$ compound, substitutions of Mo for Cu and Sr for Ba were done. Synthesis of the $YBaSrCu_{3-x}Mo_xO_{7+d}$ compound was optimized for the highest T_c and j_c. Materials prepared in air at 960 °C and annealed in 250 atm. O_2 at around 650 °C are tetragonal for $x \geqslant 0.1$. The Mo substitution on the Cu chain site increases the oxygen content above 7, and increases T_c from 81 K for $x=0$ to about 86 K for $x=0.05-0.10$. The ratio of nominal Mo content to the amount of excess oxygen is very close to 2:3 for all compositions ($0.05 \leqslant x \leqslant 0.2$) and may result from the presence of randomly distributed dimers of corner shared MoO_6 octahedra. The critical currents for the substituted samples reveal the second peak effect arising from an increased pinning force likely due to the formation of the dimers of MoO_6 octahedra in the CuO chains. The irreversibility lines show good pinning characteristics when compared to Y123.

DOI: 10.1103/PhysRevB.63.054501 PACS number(s): 74.60.Jg, 74.60.Ge, 74.62.Bf, 74.62.Dh

INTRODUCTION

Several cation substitutions were made for the small ion (copper) and for the large ions (barium and yttrium) in attempts to increase the superconducting transition temperature in $YBa_2Cu_3O_7$(Y123).[1–8] In most cases, substitutions for copper were found to rapidly decrease T_c and simultaneously influence the structural properties by decreasing the orthorhombic distortion, eventually resulting in the tetragonal structure.[1–3] For Fe and Al T_c remained constant up to 5 and 10 % substitution on the Cu-chain site, respectively.[2] A modest increase of T_c was conceivably observed by substitution of 2–5 % Co.[2] The solubility limit for Sr on the Ba site in $YBa_{2-y}Sr_yCu_3O_7$ was found around $y=1$ under normal synthesis conditions.[6] The $YBaSrCu_3O_{7+d}$ material ($y=1$), which is tetragonal for $-0.8<d<-0.4$, orthorhombic for $-0.3<d<0$, and ''average tetragonal'' for $0<d<0.3$, has not been studied in great detail so far despite the larger oxygen nonstoichiometry and richer structural properties than Y123. This lack of interest may be due to the lower maximum superconducting transition temperature $T_c \approx 82$ K for $YBaSrCu_3O_{7+d}$, $d \approx -0.1$. Recently, we have found that substitution of molybdenum for copper in $YBaSrCu_3O_{7+d}$ increases T_c to 86 K with a simultaneous structural transformation to the tetragonal structure. This inverse correlation between increasing T_c and decreasing orthorhombic distortion clearly shows that superconductivity with a high T_c is not limited to the orthorhombic structure for Y123 compounds. The observed increase of T_c is an example of improved superconducting properties of a Y123 material with the substitution of a transition element for copper.

Since $YBaSrCu_{3-x}Mo_xO_{7+d}$ materials contain a smaller strontium cation substituting for the larger barium cation in the intermediate region, it is expected that the intermediate region should be shorter than in Y123 and the molybdenum substituted materials may show improved pining properties. Moreover, molybdenum ions are expected to substitute for the chain copper and form the MoO_6 octahedra[9] which may locally perturb superconductivity in the CuO_2 plains and increase the flux pinning force by providing pinning centers. Thus, the $YBaSrCu_{3-x}Mo_xO_{7+d}$ compound is interesting for the study of irreversibility fields and critical currents.

Here, we describe optimization of the superconducting T_c, irreversibility field B_{irr}, and persistent intragrain critical current density j_p by determining the optimum composition, synthesis and annealing conditions. The structural and superconducting properties of the optimized material with the highest $T_c \approx 86$ K (achieved for $x=0.05-0.10$) are studied in detail and compared with recently published data for similar compounds.

EXPERIMENTAL DETAILS

Polycrystalline samples of $YBaSrCu_{3-x}Mo_xO_{7+d}$ with $x=0$, 0.025, 0.05, 0.075, 0.1, 0.125, 0.15, and 0.2 were synthesized from a stoichiometric mixture of oxides of Y, Mo, and Cu, and carbonates of Ba and Sr. Samples were fired in air at 880–960 °C for several days with frequent intermediate grindings. Subsequent high pressure anneals were done for

12 h in 20% O_2 in argon at a total pressure of 3 kbar (600 atm O_2 pressure) at 950–1100 °C or in pure oxygen (250–300 atm O_2) at 400–900 °C followed by slow cooling (0.2 deg./min.) to room temperature. Sample homogeneity was checked by powder x-ray diffraction. Neutron powder diffraction data were obtained using the Spatial Environment Powder Diffractometer (SEPD) at Argonne National Laboratory Intense Pulsed Neutron Source (IPNS).[10] The grain sizes and shapes were examined using a Hitachi Scanning Electron Microscope (SEM). Susceptibility and magnetization measurements were performed with a Quantum Design PPMS system. Resistivity was measured using a standard four-lead dc method.

RESULTS AND DISCUSSION

A. Synthesis and increase of T_c

Samples were fired several times at increasing temperatures, checked for phase purity, annealed under several oxygen pressures and temperatures, and checked for T_c. All studied compositions were single phase when synthesized in air at 940–960 °C. Small amounts of impurities (<3%) were present for synthesis temperatures lower than 940 °C due to incomplete reaction. Partial melting and small amounts of impurity phases were observed for temperatures higher than 960 °C. High pressure oxygen anneals at temperatures around 650 °C followed by slow cooling were found to be the optimal way to increase of the oxygen content and to obtain the highest T_c. For the optimized oxygen anneal, the best samples were obtained when the first synthesis step was made just below the melting temperature at 960 °C. Small amounts of calcium, less then 10%, can be substituted for yttrium resulting in a material with lower T_c. The $x=0$, 0.05, 0.10, and 0.20 materials prepared in air at 960 °C and annealed in high oxygen pressure were chosen for structural and superconducting characterization. Samples with $x=0$ and 0.1 were annealed in 300 atm O_2 at 700 °C. Samples with $x=0.05$ and 0.20 were annealed in 250 atm O_2 at 600 and 700 °C, respectively. Small differences of the annealing conditions among samples (pressure, 250–300 atm; temperature, 600–700 °C) were not important for the overall oxygen content and crystallographic structure but affected slightly the intergrain superconducting properties.

The highest $T_c \approx 86$ K was observed for $x=0.05-0.1$ samples annealed at high oxygen pressure. For samples annealed at 1 atm O_2 the highest $T_c \approx 82$ K was seen for $x=0-0.05$. Anneals at lower oxygen pressure $P(O_2)=0.01$ atm, quickly decreased T_c ($T_c \approx 45$ K for $x=0$) and broadened the transitions. Figure 1 shows normalized resistivity for three single phase samples which were annealed in oxygen at 1 atm [Fig. 1(a)] and high pressure [Fig. 1(b)]. Clearly, T_c is a function of both the doping level x and the oxygen content d. The sample with $x=0$ does not change T_c significantly after the high oxygen pressure treatment. Superconducting transitions for optimally doped and annealed $YBaSrCu_{3-x}Mo_xO_{7+d}$ samples are very sharp, indicating good quality of our material [see inset in Fig. 1(b)]. T_c's for samples with $x=0.05-0.10$ are higher than for $YBaSrCu_3O_{7+d}$. This is an example of a notable increase of T_c for a Y123 material by substitution of a transition element for copper.

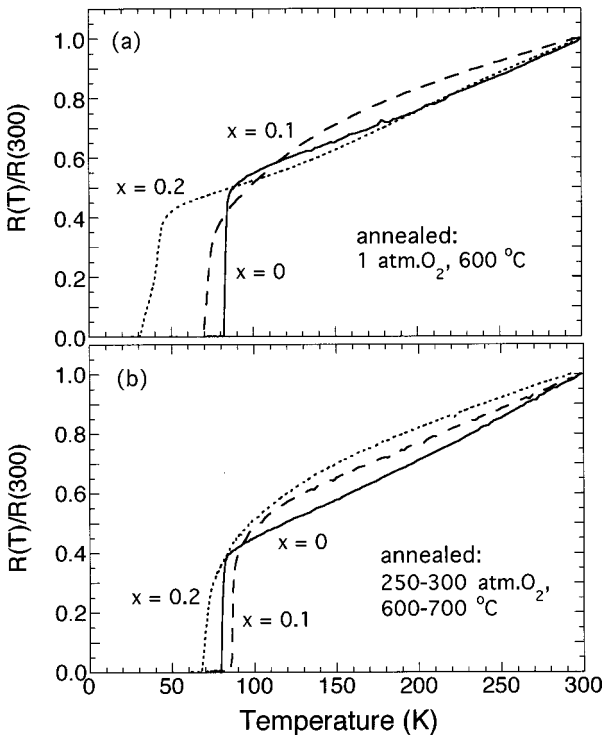

FIG. 1. Normalized resistance as a function of temperature for the $YBaSrCu_{3-x}Mo_xO_{7+d}$ samples with $x=0$, 0.1, and 0.2, as prepared (a) and after the high oxygen pressure anneal (b). The superconducting transition temperature for the nonsubstituted sample is only insignificantly affected by the high pressure anneal.

The normal state resistivity displays a complicated temperature behavior that depends on both x and d. For example, the temperature dependencies of the resistivity for the $x=0.2$ sample annealed at 250 atm O_2 and for the $x=0.1$ sample annealed in 1 atm O_2 show behavior typical of underdoped materials. For both samples, on cooling from temperatures much higher then T_c, there is a gradual decrease of resistivity from linear dependence. To relate this behavior to the pseudogap or the c-axis transport properties would require the study of single crystals, which are not available at present.

SEM measurements were performed to determine the shapes and sizes of the grains for all our samples. For Mo-free material, the grains have approximately spherical shape, are well connected, and have a size distribution ranging from 1 to 6 μm, with most of grains having diameters of about 3 μm. For Mo-substituted materials, the small grains are approximately spherical but the largest grains have more platelike shapes. The grains are well connected and have a size distribution between 1 and 9 μm, with most of the grains having dimensions of about 4 μm. Thus, to estimate the effective superconducting volume fraction of the grains and to evaluate the critical persistent-currents, an average grain size 3 and 4 μm was taken for the nonsubstituted and Mo-substituted samples, respectively.

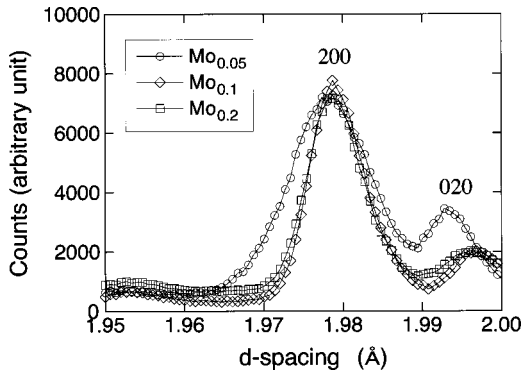

FIG. 2. Neutron diffraction data near the 200/020 peak for several Mo-substituted samples. The broadening of the peak for the $x=0.05$ sample indicates the orthorhombic splitting.

B. Structure and oxygen content

Neutron powder diffraction data were collected for ~3 g samples at room temperature on the Special Environment Powder Diffractometer (SEPD) at Argonne's Intense Pulsed Neutron Source (IPNS).[10] The raw data show no impurity phases. Structural parameters were refined using the General Structural Analysis Software (GSAS) suite of programs.[11] Only data from the high-resolution backscattering detector banks ($\Delta d/d \approx 0.035$) were used in the refinements. Initial refinements showed that the $x=0.05$ sample crystallizes in an orthorhombic space group *Pmmm* while the $x \geqslant 0.1$ samples crystallize in the tetragonal space group $P4/mmm$. Figure 2 shows diffraction data near the 200/020 diffraction peak for several samples. The broadening of the 200/020 peak for the $x=0.05$ sample indicates a small orthorhombic splitting. Figure 3 shows the diffraction data and the best-fit Rietveld profile for the $x=0.2$ sample. The substituted Mo was found to occupy solely the chain site. Ba and Sr were found to share the Ba site. During the refinements, Ba and Sr ions were allowed to have different *z* coordinates. The coordinates were found to differ by 0.14–0.21 Å. Since the neutron diffraction patterns showed no impurities, the cationic compositions were fixed at their nominal values.

The oxygen atoms in the CuO_2 plane, O(1) and O(2), were found to show a typical displacement pattern towards the Y site. The O(1) and O(2) occupancies refined to approximately 2.0. The apical oxygen atom O(3) was found to have a large thermal factor owing to the smaller size of the Sr ion and its displaced position. The value of this thermal factor was reduced by displacing the apical oxygen atom from its initial position [from $(0\ 0\ z)$ to $(x\ y\ z)$; $x \neq y$ for the $x=0.05$ sample and $x=y$ for the $x=0.1$ and 0.2 samples]. The site fraction of O(3) was refined to about 0.25 for all samples studied, indicating that the site is fully occupied. Consequently, the O(1), O(2), and O(3) occupancies were not refined.

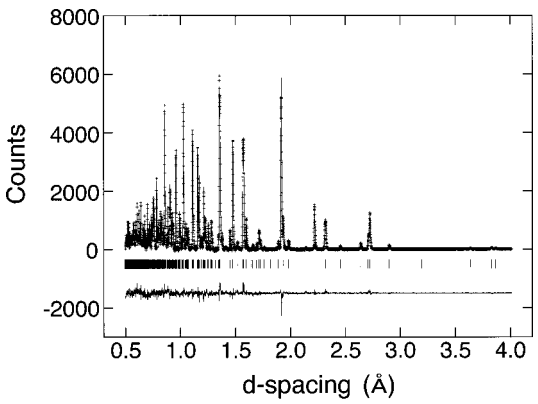

FIG. 3. Neutron diffraction data and the best-fit Rietveld profile for the $x=0.2$ sample.

The $Cu_{1-x}Mo_xO_y$ chain is situated between the two (Ba, Sr) layers in the intermediate region of the structure. Consequently, individual chain oxygen atoms observe different arrangements of the neighboring Sr and Ba atoms and the Cu and Mo atoms leading to local static displacements. It is, thus, difficult to determine their precise locations. However, the dominant average positions can be refined. For instance, the oxygen atoms are found to occupy two independent sites $(\frac{1}{2}\ y\ 0)$ and $(x\ \frac{1}{2}\ 0)$ in the orthorhombic $x=0.05$ compound. Their occupancies are refined as 0.59 and 0.48, respectively, with the site occupancy difference being consistent with the orthorhombic distortion. For the $x=0.1$ and 0.2 tetragonal samples, the occupancies of these sites become equal by symmetry because the positions are equivalent. However, a splitting of oxygen atoms into ideal and displaced sites, $(\frac{1}{2}\ 0\ 0)$ and $(\frac{1}{2}\ x\ 0)$, is observed.

The total refined oxygen contents that were obtained from the refined oxygen occupancies are 7.07 ± 0.02, 7.16 ± 0.04, and 7.30 ± 0.04 for the $x=0.05$, 0.1, and 0.2 samples, respectively. Notably, the ratio of nominal Mo to the amount of excess oxygen in the blocking layer (i.e., 0.07, 0.16, and 0.30) is very close to 2:3 in all three samples. This ratio could arise from the presence of the randomly distributed dimers of corner shared MoO_6 octahedra in a fashion similar to that observed for $YSr_2Cu_{3-x}M_xO_z$ $(M=\mathrm{Mo, W})$.[12] The oxygen contents are approximately equal to those expected for replacing chain Cu^{3+} with Mo in its highest allowed oxidation state 6+ consistent with the preparation conditions. Table I gives a summary of the refined structural coordinates for $x=0.05$, 0.1, and 0.2 samples; selected interatomic bond lengths are given in Table II.

The schematic structure of structurally similar double-CuO_2-plane compounds with a single metal-oxygen layer in the intermediate region is shown in Fig. 4. These compounds can be described in terms of the inter-CuO_2-plane distance *d*(inter), which defines the thickness of the intermediate region, and the intra-CuO_2-plane distance *d*(intra), which denotes the thickness of the block of CuO_2 planes. The sum of these two distances is equal to the *c*-axis lattice constant. The thickness of the blocking layer *d*(block), where Mo is substituted for the chain-site Cu, is defined as twice the Cu/Mo(1)-O(3) bond length. This region is thought to have a critical effect on the *c*-axis normal state and superconducting properties of several high-temperature superconductors. The relevant distances and the superconducting T_c's are given in Table III for three optimally doped Y123 compounds $YBa_2Cu_3O_7$, $YBaSrCu_{2.9}M_{0.1}O_{7.16}$, and $YSr_2Cu_{2.8}M_{0.2}O_{7.3}$.

TABLE I. Refined structural parameters for $YBaSrCu_{3-x}Mo_xO_{7\pm\delta}$.

Atom Space group		$x=0.05$ *Pmmm*	$x=0.1$ *P4/mmm*	$x=0.2$ *P4/mmm*
a (Å)		3.82635(7)	3.82210(3)	3.83072(4)
b (Å)		3.81263(7)		
c (Å)		11.5558(2)	11.5754(1)	11.5984(2)
Y	*at* ($\frac{1}{2}$ $\frac{1}{2}$ $\frac{1}{2}$)			
	B (Å^2)	0.51(3)	0.46(3)	0.52(3)
Ba/Sr	*at* ($\frac{1}{2}$ $\frac{1}{2}$ z)			
	z (Ba)	0.1922(8)	0.1959(5)	0.1981(6)
	z (Sr)	0.1799(6)	0.1788(4)	0.1801(4)
	B (Å^2)	0.93(5)	0.81(4)	0.81(5)
Cu1/Mo	*at* (0 0 0)			
	B (Å^2)	1.24(4)	1.14(4)	1.18(4)
Cu2	*at* (0 0 z)			
	z	0.3535(1)	0.3537(1)	0.3551(1)
	B (Å^2)	0.60(2)	0.47(2)	0.43(2)
O1	*at* ($\frac{1}{2}$ 0 z)			
	z	0.3733(3)	0.37627(9)	0.3766(1)
	B (Å^2)	0.40(5)	0.58(2)	0.59(2)
O2	*at* (0 $\frac{1}{2}$ z)			
	z	0.3788(4)		
	B (Å^2)	0.80(6)		
O3	*at* (x y z)			
	x	0.027(2)	0.0367(8)	0.0374(9)
	y	0.042(1)	0.0367(8)	0.0374(9)
	z	0.1595(2)	0.1595(2)	0.1597(2)
	B (Å^2)	0.56(6)	0.52(6)	0.50(6)
	n	0.25	0.25	0.25
O4	*at* (x $\frac{1}{2}$ 0)			
	x	0.134(3)	0.160(3)	0.156(3)
	B (Å^2)	1.3(1)	1.3(1)	1.4(1)
	n	0.48(1)	0.60(2)	0.66(2)
O5	*at* ($\frac{1}{2}$ y 0)			
	y	0.062(3)	0	0
	B (Å^2)	1.3(1)	1.3(1)	1.4(1)
	n	0.59(1)	0.56(2)	0.63(2)
R_p (%)		4.17	3.61	3.50
R_{wp} (%)		6.03	5.21	5.46
c^2		2.435	1.561	1.366

A systematic decrease of T_c is associated with the shortening of the apical bond-length of the planar Cu, d(apical), as has been observed for several structurally similar compounds.[13,14] The $YBaSrCu_{2.9}M_{0.1}O_{7.16}$ compound has the middle d(apical) and, thus, the middle T_c. The thickness of the intermediate region d(inter), is for that compound also between values observed for $YBa_2Cu_3O_7$ and $YSr_2Cu_{2.8}M_{0.2}O_{7.3}$.

C. Superconducting properties

Superconducting properties were studied by ac susceptibility χ and dc magnetization M in the temperature range from 5 to 100 K using applied fields from 0 to 7 T. Solid pieces as well as powdered samples with masses of about 100 mg were used for both χ and M measurements. The susceptibility was measured upon warming from the zero-field-cooled (ZFC) state using the ac field of 1 Oe at 200 Hz. For solid samples, measured at zero dc field, the 1 Oe ac field was large enough to separate the higher-T_c intragrain and lower-T_c intergrain components for the $x=0.05$ sample, but was not sufficient to show clear intragrain and intergrain shielding properties for the $x=0$ and 0.1 samples. The differences in shielding properties may result from slightly different annealing conditions used for those materials. Figure 5 shows the real part of the ac susceptibility χ' as a function of temperature measured at several dc fields for two Mo-substituted samples. The weaker intergrain shielding for the $x=0.05$ sample is clearly observed for zero and 1–7 T dc fields as a second hump and smaller shielding fraction, respectively. For the $x=0.05$ sample, the coupling between grains is destroyed in fields larger than 1 T at temperatures above 40 K. For the sample with $x=0.1$, annealed at slightly higher oxygen pressure and temperature, some intergrain shielding is present even at a 7 T field indicating much stronger coupling between grains. Similar good intergrain coupling was also observed for the $x=0$ sample.

Calculation of the intragrain persistent critical currents from the magnetization loops requires removal of the intergrain contribution to the diamagnetic signal. Therefore, the solid pieces of samples were powdered and susceptibility was measured again. For these powdered samples, the intergrain properties were not observed at any temperatures above 5 K for fields above 1 T. Thus, powder samples were used to measure the intragrain critical currents. However, both the powder and solid samples were exploited to study the intragrain irreversibility fields.

The shielding effect and the effective superconducting volume fraction of grains were estimated from the ac susceptibility measurements performed at 5 K. The average density of the solid samples was measured to be ≈ 4.8 (± 0.1) g/cm^3; i.e., about 80% of the theoretical material density (6.1 g/cm^3). The absolute χ' values were obtained using the measured sample volume and correcting the data by taking demagnetizing effects into account. For our solid samples, the demagnetizing factor N is about 0.13. At 5 K and zero dc field, the corrected χ' values for all solid samples ($x=0$, 0.05, and 0.1) are about 5% lower than the ideal value, $-1/4\pi$, indicating almost perfect shielding, as expected.

The effective superconducting volume fraction of grains v can be estimated for both solid and powder samples when the grains are decoupled in magnetic fields that are large enough to depress superconductivity in the intergrain region. For example, for the $x=0.05$ solid sample, $\chi'(T)$ measured in a 7 T field between 40 and 50 K [see Fig. 5(a)] can be extrapolated to 5 K and used to estimate v. For that reason, the sample material volume was calculated from the sample mass and theoretical material density. The approximate correction for the grain demagnetizing factor was made assuming a more spherical ($N\approx 0.33$) than the platelike shape of the grains. Then, taking into account the magnetic penetration depth $\lambda \approx 0.2\,\mu$m, which decreases the ac-field-screened

TABLE II. Selected bond lengths (Å) for $YBaSrCu_{3-x}Mo_xO_{7\pm\delta}$.

Distance	$x=0.05$	$x=0.1$	$x=0.2$
Y-O1	2.404(2)	2.3882(7)	2.3911(7)
Y-O2	2.371(2)		
Ba-Sr	0.14(2)	0.20(1)	0.21(1)
Ba-O1	2.831(8)	2.830(5)	2.820(5)
Ba-O2	2.882(8)		
$Ba\text{-}O3_{ave}$	2.731(7)	2.739(3)	2.749(3)
Ba-O4	2.625(9)/3.290(12)	2.613(8)/3.394(10)	2.649(8)/3.263(4)
Ba-O5	2.779(11)	2.966(5)	2.992(5)
Sr-O1	2.938(6)	2.979(3)	2.977(4)
Sr-02	2.991(6)		
$Sr\text{-}03_{ave}$	2.714(7)	2.715(5)	2.723(5)
Sr-O4	2.506(10)/3.196(10)	2.443(8)/3.265(9)	2.469(8)/3.268(10)
Sr-O5	2.666(8)	2.817(3)	2.834(3)
(Cu1, Mo)-O3	1.853(2)	1.857(2)	1.863(2)
(Cu1, Mo)-O4	1.974(3)	2.007(4)	2.007(4)
(Cu1, Mo)-O5	1.928(1)	1.91105(2)	1.91536(2)
Cu2-O1	1.9268(5)	1.9288(2)	1.9316(2)
Cu2-O2	1.9286(7)		
Cu2-O3	2.250(2)	2.257(2)	2.275(2)

volume and is only about 15–20 times smaller than the average grain diameter, the effective superconducting volume fraction of grains for the solid sample is computed to be $v \approx 70\%$. This value may be slightly overestimated, because for the solid samples some clusters of the nonseparated grains may still exist even in high magnetic fields.

For powder samples, a complete grain separation is observed in a 1 T field at temperatures down to 5 K. χ' is equal to about 0.026 emu/cm^3 Oe for all three compositions when, as above, the material volume is calculated from the measured sample mass and the theoretical material density, and an approximate correction is made for the grain demagnetizing factor ($N \approx 0.33$). Then, after taking into consideration the magnetic penetration depth $\lambda \approx 0.2\,\mu$m, the effective superconducting volume fraction of grains for the powder samples is found to be $v \approx 45\%$. This value is underestimated because it has been calculated for the mean size of the grains, whereas the ''λ effect'' influences smaller grains more than larger grains (different λ/grain-radius ratio). Consequently, the relatively high effective superconducting volume fraction of grains was found to be between 45 and 70 %. This confirms bulk superconductivity and, moreover, attests to the good quality of our compound when compared with pure Y123 ($v \approx 70\%$).[15]

The irreversibility fields B_{irr}^{ac} and B_{irr}^{dc} were obtained from ac susceptibility and dc magnetization measurements, respectively. The irreversibility lines $B_{irr}^{ac}(T)$ were derived from $\chi(T)$ curves measured at constant dc fields (see Fig. 5). Each irreversibility point $(B_{irr}^{ac}, T_{irr}^{ac})$ was obtained by measuring the temperature at which the imaginary part of the ac susceptibility χ'' begins to differ from zero. Below the temperature T_{irr}^{ac} both the critical current and ac losses differ from zero, i.e. the magnetization is irreversible. So, the defined T_{irr}^{ac} corresponds to a temperature where resistivity is zero and the diamagnetic signal appears for the real part of the ac susceptibility χ'. More generally, the $B_{irr}^{ac}(T)$ lines are the upper bound for the $B_{irr}^{dc}(T)$ lines that are highly dependent on the measurement sensitivity. The $B_{irr}^{dc}(T)$ lines were determined by measuring the fields at which magnetic hysteresis for the $M(B)$ loops disappears at constant temperature. Additional points for the $B_{irr}^{dc}(T)$ lines were obtained by measuring the temperatures at which the $M(T)$ curves split when measured at constant field for zero-field-cooled and field-cooled samples. In both cases the criterion used was $\Delta 4\pi M = 0.05$ G.

Irreversibility lines determined from both susceptibility $B_{irr}^{ac}(T)$, and magnetization $B_{irr}^{dc}(T)$, are shown in Fig. 6 for

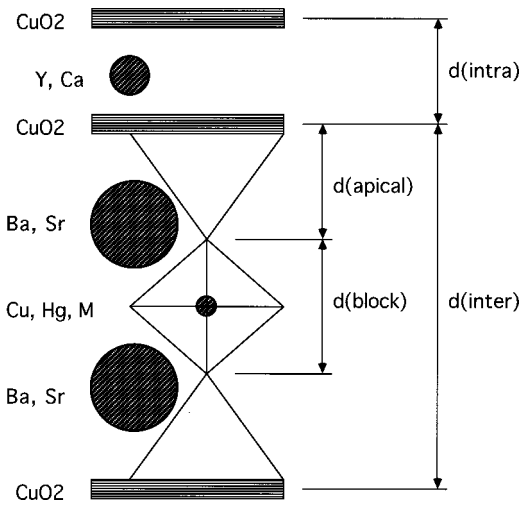

FIG. 4. Schematic structure of the double-CuO_2-plane compounds with a single metal-oxygen layer in the intermediate region (Ref. 12).

TABLE III. The relevant distances (see Fig. 4) and superconducting T_C's for the optimally doped $YBa_2Cu_3O_7$, $YBaSrCu_{2.9}Mo_{0.1}O_{7.16}$, and $YSr_2Cu_{2.8}Mo_{0.2}O_{7.3}$.

		$YBa_2Cu_3O_7$	$YBaSrCu_{2.9}Mo_{0.1}O_{7.16}$	$YSr_2Cu_{2.8}Mo_{0.2}O_{7.3}$
c	(Å)	11.680	11.575	11.486
d(intra)	(Å)	3.373	3.347	3.378
d(inter)	(Å)	8.307	8.228	8.108
d(block)	(Å)	3.700	3.714	3.698
d(apical)	(Å)	2.303	2.257	2.205
T_C	(K)	93	86	75

$YBaSrCu_{3-x}Mo_xO_{7+d}$ with $x=0$, 0.05, and 0.1 for solid and powder samples. The highest irreversibility lines and the largest slopes $dB_{\rm irr}/dT$, that may indicate the strongest flux pinning, were obtained for samples with $x=0.05$. For those samples, the strongest flux pinning is evident in the similar position of the $B_{\rm irr}^{\rm dc}(T)$ and $B_{\rm irr}^{\rm ac}(T)$ lines on the $B_{\rm irr}$-T diagram (see Fig. 6). The similarity of the irreversibility lines occurs because the strong pinning force that sharpens the transition from liquid to solid vortex states simultaneously softens the dependence of the irreversibility point $(B_{\rm irr},T)$ on the voltage criterion and, therefore, also on the measurement technique used. The smallest $dB_{\rm irr}/dT$ and the largest divergence between $B_{\rm irr}^{\rm dc}(T)$ and $B_{\rm irr}^{\rm ac}(T)$ lines are seen for the $x=0.1$ sample. The most likely reason for decreased pinning may be poorer coupling of the CuO_2 planes through the less metallic blocking layer. It appears that 10% substitution of Mo for Cu in the chains introduces too much disorder that decreases the pinning properties when compared with the $x=0$ and 0.05 samples, despite the higher T_c of the $x=0.1$ sample.

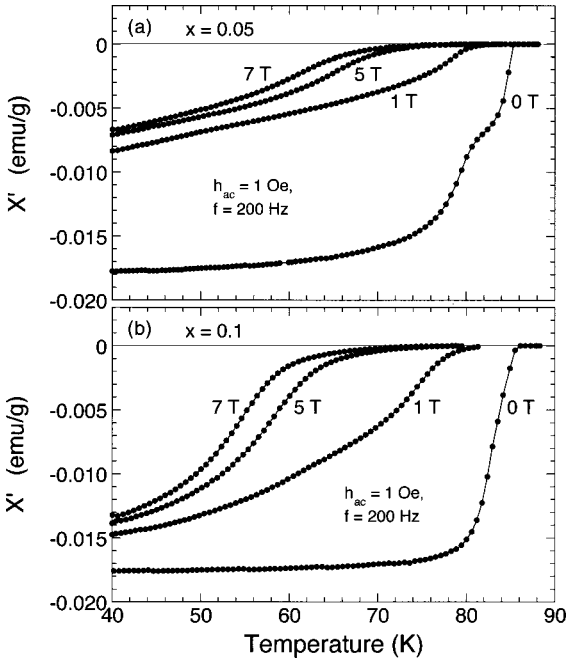

FIG. 5. Real part of the ac susceptibility χ' versus temperature for the $x=0.05$ (a) and 0.1 (b) solid samples measured at 0, 1, 5, and 7 T magnetic fields. Strong intergrain coupling is observed for the sample with $x=0.1$ annealed at slightly higher temperature.

The enhanced pinning properties for the material with $x=0.05$ are better displayed when the $B_{\rm irr}$ fields are plotted as a function of reduced temperature $t=T/T_c$ as presented in Fig. 7. The $B_{\rm irr}(t)$ line for the $x=0.05$ sample is about 1 T above the line for the $x=0$ sample and is very close to the line obtained for polycrystalline pure Y123.[16] In Fig. 7, the $B_{\rm irr}(t)$ lines for polycrystalline Hg1201 (Ref. 17) and single crystals of Bi2212, LSCO, and Y123 (Ref. 18) are also presented. The single crystal data are shown to provide a comparison with results that are free of extrinsic pinning. Moreover, the single crystals were measured in fields parallel to the c axis, i.e., in the direction of the weakest intrinsic flux pinning. Therefore, the results for single crystals are expected to show lower irreversibility lines $B_{\rm irr}$ than are obtained for polycrystalline material for which the applied field is randomly oriented with respect to the crystal axes.

The Mo ions substituted for Cu in the CuO chains most likely influence the superconducting properties in at least three ways. First, they act as doping elements decreasing the hole concentration. This doping is compensated by excess oxygen above 7 introduced into the chain region of the structure. Second, the Mo-created local structural distortions may, on average, increase the Cu/Mo(1)-O(3) bond length and, therefore, elevate T_c. Third, Mo ions may work as elements creating pinning centers by forming the randomly distributed dimers of corner sharing MoO_6 octahedra, introducing extended distortions and, therefore, perturbing locally superconductivity in the CuO_2 planes. The isolated perturbation

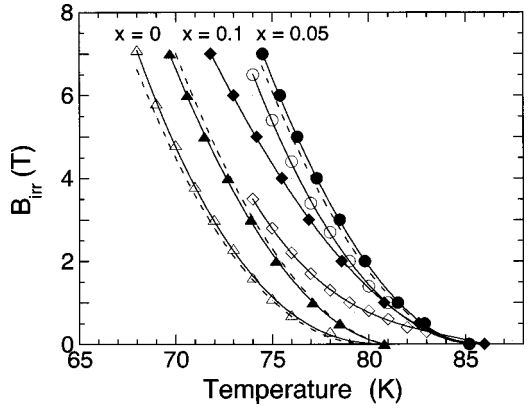

FIG. 6. Irreversibility fields $B_{\rm irr}$ obtained as a function of temperature by dc (open symbols) and ac (closed symbols) techniques for the $x=0$ (triangles), 0.05 (circles), and 0.1 (diamonds) solid samples (solid lines) and powders (broken lines).

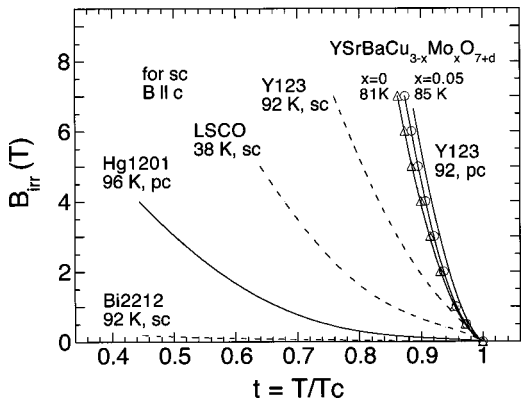

FIG. 7. Irreversibility fields as a function of reduced temperature for $YBaSrCu_{3-x}Mo_xO_{7+d}$ samples with $x=0$ (triangles) and 0.05 (circles); Y123 (Ref. 16) and Hg1201 (Ref. 17) polycrystalline materials (pc: solid lines); Bi2212, LSCO, and Y123 single crystals (Ref. 18) (sc. broken lines). The data for single crystals is for B parallel to the c axis. The superconducting transition temperature is displayed for each compound.

with a dimension of 2–3 unit cells in the *ab* plane is comparable to the superconducting coherence length ξ, and therefore may act as a pinning center. Assuming a roughly homogeneous distribution of the dimers of MoO_6 octahedra, the distance between them is on the average 3–4 unit cells for the $x=0.05$ sample, i.e., $\approx$11–15 Å in the *ab* plane. The distance between pinning centers in the *ab* plane is crucial to pin vortices in the case of the $B\|c$ axis. For the $B\perp c$ axis, the CuO_2 layers, being quasi-two-dimensional pinning centers, work much more effectively than the quasi-zero-dimensional dimers of MoO_6 octahedra. Possible ordering of the randomly distributed dimers along the c axis would form more effective quasi-one-dimensional pinning centers, as was proposed for $Hg_{1-x}Cr_xSr_2CuO_4$.[14,19] The relatively short distance between the MoO_6 dimers does not match the distance between vortices in a vortex lattice for any reasonable high dc field and the dimers cannot work as perfect pinning centers. However, clear evidence for the significant increase of the pinning force was observed for the $B_{\rm irr}(T)$ lines measured for the $x=0.05$ sample when compared with the $x=0$ material.

To determine the critical persistent-current density j_p the magnetization loops $M(B)$ were measured at constant temperature for powder samples. The Bean formula was used to calculate $j_p(A/\mathrm{cm}^2)=k\Delta M/w$, where M is in emu/cm^3, w is a scaling length in cm, and k is a shape coefficient. The formula was applied only in the range of magnetic fields where M was weakly field dependent, i.e., above the first peak observed for the $M(B)$ curves. The grain diameter was used as the size of the current loops w for dc fields high enough to separate grains, as it results from the ac susceptibility measured at various dc fields (see Fig. 5). The separation of grains was confirmed by the absence of a second maximum in the $\chi''(T)$ measurements that would mark the transition to the superconducting state for the intergrain material. The grain decoupling field B_d was about 1 T at the decoupling temperature $T_d\approx$60, 55, and 50 K for the $x=0$, 0.05, and 0.1 powder samples, respectively. The superconducting magnetic and transport properties can be significantly influenced by intergrain coupling for fields smaller than B_d or temperatures below T_d. Consequently, the scaling length w and persistent critical current cannot be determined unambiguously below B_d or T_d. As revealed by ac susceptibility measurements for our powder samples, the intergrain coupling is small even at 5 K for fields above 1 T. Thus, we can conclude that for fields above 1 T the intergrain component of j_p can be neglected at any temperature.

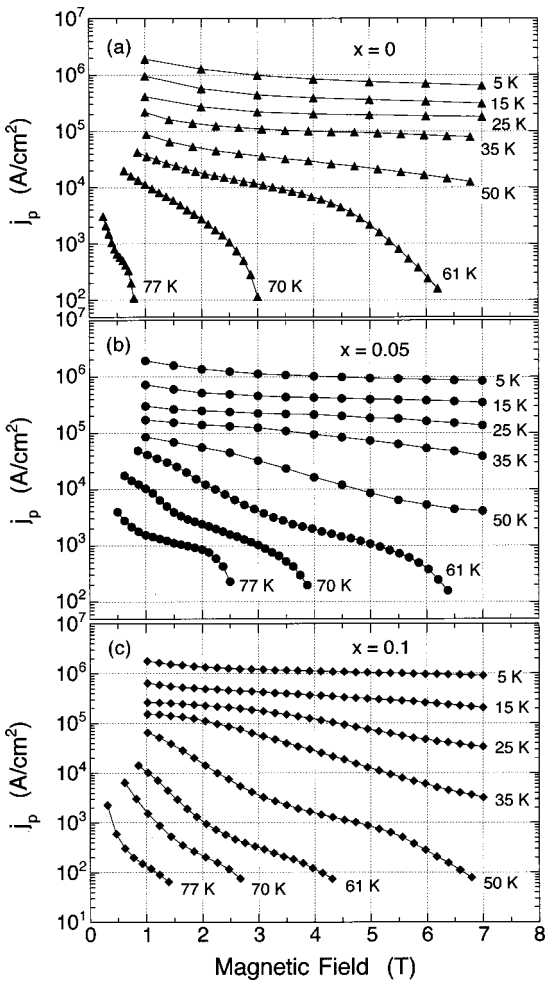

FIG. 8. Critical persistent-currents j_p versus magnetic field at several temperatures for the $YBaSrCu_{3-x}Mo_xO_{7+d}$ samples with $x=0$ (a), 0.05 (b), and 0.1 (c). The second peak effect is observed for the substituted compound only.

The intragrain j_p was determined assuming nearly spherical grains ($k=40$), and taking $w=3$, 4, and 4 μm as an average grain diameter for the $x=0$, 0.05, and 0.1 samples, respectively. Figure 8 shows j_p as a function of B for these compositions at several temperatures between 5 and 77 K. At 5 K, j_p is about $10^6 A/\mathrm{cm}^2$ and almost independent of B for all three compositions. Similar values of j_p arise because at low temperatures the coherence length in the c-axis direction ($\xi_c\approx$3–4 Å) is comparable to the d(block) distance for all compounds, i.e., the blocking region between superconducting CuO_2 planes may act as a strong intrinsic pinning center. However, differences in $j_p(B)$ among pure and Mo-substituted samples are expected at higher temperatures

where ξ increases and other types of pinning centers with more extended dimensions should act more effectively.

Figure 8(a) shows that for the $x=0$ sample there are three regions of j_p dependence on B. At low fields, j_p decreases faster than exponentially for all temperatures, similar to other high-temperature superconductors. At higher fields, an exponential dependence is observed, which below 25 K extends to fields of at least 7 T. At higher temperatures, the range of exponential dependence is narrowed and followed by a more rapid decrease, especially above 60 K. No sign of the second peak effect in the form of a positive deviation from the exponential dependence of $j_p(B)$ is observed for the $x=0$ sample.

Figure 8(b) shows that for the $x=0.05$ composition the region of the exponential decrease is more narrow and shifted to lower fields for all temperatures suggesting a weaker pinning force at low fields for the Mo-substituted sample. However, at higher fields a positive deviation of $j_p(B)$ from the exponential dependence is observed. For example, at 50 K the exponential $j_p(B)$ dependence extends from 1 to 3 T and is followed by a more rapid decrease between 3 and 5 T. The decrease is suppressed in fields above 5 T and then j_p is almost field independent for fields around 7 T. This behavior, frequently called the second peak effect, is even more pronounced at higher temperatures. The critical currents above 70 K are much larger for the sample with $x=0.05$ than for that with $x=0$. At small fields it is probably a result of a higher T_c for the $x=0.05$ sample. For fields above 1 T the increased j_p is apparently the result of an enhanced pinning force caused by introducing of the MoO_6 dimers.

Figure 8(c) shows that $j_p(B)$ for the $x=0.1$ sample displays features similar to those observed for the $x=0.05$ sample. However, both pinning at low fields and the second peak effect are weaker for the $x=0.1$ composition, as seen by a more rapid decrease of $j_p(B)$ with increasing temperature. For example, at 50 K the exponential $j_p(B)$ dependence extends only to 1.5 T, and is followed by a more rapid decrease between 1.5 and 3 T. This decrease is somewhat suppressed for fields between 3 and 5 T, and finally a rapid decrease is observed again above 5 T. Thus, the second peak effect for the $x=0.1$ sample is present only at a much smaller field range than for the $x=0.05$ composition.

The $j_p(B)$ curves close to T_c are compared in Fig. 9 for all three compositions. At 70 K and for fields above 2.2 T, the $j_p(B)$ for the $x=0.05$ sample is the largest. Clearly, the reason for the largest pinning force is the second peak effect observable for $B\approx 1.5-3.5$ T. At higher temperatures, the second peak effect is even more pronounced for $B\approx 1.0-2.2$ T, where $j_p(B)$ for the $x=0.05$ sample at 77 K is larger than that for the $x=0$ sample at 70 K. The $x=0.1$ composition has clearly the weakest intrinsic pinning at 70 K. However, at 77 K and low fields the $j_p(B)$ for this composition is similar to that for the $x=0$ sample, probably as the result of higher T_c observed for the $x=0.1$ composition.

The second peak effect, present for both Mo-substituted samples, can be explained assuming the temperature dependence of the coherence length, e.g., $\xi_{ab,c}\sim(1-t)^{-1/2}$. As ξ_c increases with increasing temperature, types of pinning centers other than the blocking region between the double CuO_2 planes can be important for increasing j_p. For the Mo-substituted samples, the MoO_6 dimers locally perturbing superconductivity are likely to be the pinning centers at elevated temperatures. An additional increase of the pinning force is possible if more extended regions of superconducting CuO_2 planes would be perturbed and the distance between them would increase. Both effects would improve the pinning properties, especially at higher temperatures where ξ_{ab} extends for more than several unit cells. Thus, two pinning mechanisms control the critical current for our Mo-substituted samples. With increasing temperature, the first type of pinning, caused by the blocking region between the double CuO_2 planes, becomes weaker, but simultaneously the second type of pinning, caused by the MoO_6 dimers or clusters, strengthens and then decays close to T_c. Superposition of these two pinning mechanisms most likely results in the second peak effect observed for our samples.

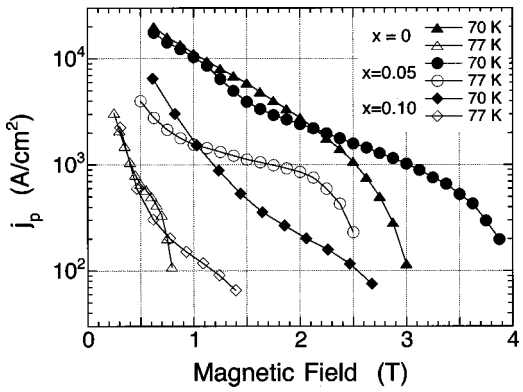

FIG. 9. Critical persistent currents versus magnetic field at 70 K (closed symbols) and 77 K (open symbols) for the $YBaSrCu_{3-x}Mo_xO_{7+d}$ samples with $x=0$ (triangles), 0.05 (circles), and 0.1 (diamonds). The second peak effect is the clear reason for larger critical currents obtained for the $x=0.05$ sample when compare to the critical currents for the nonsubstituted compound.

CONCLUSION

Synthesis conditions and compositions were optimized for the $YBaSrCu_3O_7$ superconductor, where smaller Sr is substituted for larger Ba to decrease the distance between the superconducting blocks of double CuO_2 planes. The highest T_c was obtained by substituting Mo to the CuO chain in the blocking layer and after a high oxygen pressure anneal that preserves good contacts between grains if it is done at high enough temperature. The Mo-substituted material $YBaSrCu_{3-x}Mo_xO_{7+d}$, with $x=0.05$ has $T_c=85$ K and exhibits excellent intrinsic pinning properties when compared with other high-temperature superconductors. The scaled $B_{\rm irr}(t)$ lines for the composition with $x=0.05$ and pure Y123 are similar. However, in the absolute temperature scale $B_{\rm irr}(T)$ is worse for the $x=0.05$ sample because of lower T_c by 6 K. The intrinsic pinning properties of this substituted material are significantly modified most likely by formation

of the MoO_6 octahedra dimers. The dimers may locally perturb superconductivity on the superconducting coherence length scale and therefore can act as effective pinning centers. A clear evidence for the increased pinning force was found from a second peak effect present in the $j_p(B)$ dependence for the Mo-substituted material, while the effect was not observed for the $x=0$ sample. More extensive clustering of the MoO_6 octahedra may be required to further improve the pinning characteristics for the substituted material. In addition, a smaller substitution amount may be favorable since it would increase the distance between the clusters, and thus may provide better matching of the pinning center lattice and the vortex lattice and thereby additionally enhance the pinning force.

ACKNOWLEDGMENTS

This work was supported by the TMR Network under Contract No. ERBFMRX-CT98-0189 (K.R.), the National Science Foundation Science and Technology Center for Superconductivity under Grant No. DMR 91-20000 (B.D., O.C.), and the U.S. Department of Energy, BES-Materials Sciences under Contract No. W-31-109-ENG-38 (J.D.J.).

[1] T. Siegrist, L. F. Schneemeyer, J. V. Waszczak, N. P. Singh, R. L. Opila, B. Batlogg, L. W. Rupp, and D. W. Murphy, Phys. Rev. B **36**, 8365 (1987).

[2] J. M. Tarascon, P. Barboux, P. F. Miceli, L. H. Greene, G. W. Hull, M. Eibschutz, and S. A. Sunshine, Phys. Rev. B **37**, 7458 (1988); P. F. Miceli, J. M. Tarascon, I. H. Greene, P. Barboux, F. J. Rotella, and J. D. Jorgensen, *ibid.* **37**, 5932 (1988).

[3] Gang Xiao, M. Z. Cieplak, A. Gavrin, F. H. Streitz, A. Bakhshai, and C. L. Chien, Phys. Rev. Lett. **60**, 1446 (1988).

[4] T. Wada, Y. Yaegashi, A. Ichinose, H. Yamauchi, and S. Tanaka, Phys. Rev. B **44**, 2341 (1991).

[5] M. W. Shafer, T. Penney, B. L. Olson, R. L. Greene, and R. H. Koch, Phys. Rev. B **39**, 2914 (1989).

[6] B. W. Veal, W. K. Kwok, A. Umezawa, G. W. Crabtree, J. D. Jorgensen, J. W. Downey, L. J. Nowicki, A. W. Mitchell, A. P. Paulikas, and C. H. Sowers, Appl. Phys. Lett. **51**, 279 (1989).

[7] S. Li, E. A. Hayri, K. V. Ramanujachary, and M. Greenblatt, Phys. Rev. B **38**, 2450 (1988).

[8] R. A. Gunasekaran, B. Hellebrand, and P. L. Steger, Physica C **270**, 25 (1996).

[9] B. Dabrowski, K. Rogacki, O. Chmaissem, J. D. Jorgensen, J. W. Koenitzer, and K. R. Poeppelmeier, in *Proceedings of the Third European Conference on Applied Superconductivity (EUCAS'97)*, The Netherlands, Institute of Physics Conference Series No. 158 edited by H. Rogalla and D. H. A. Blank (IOP Publishing, Bristol, 1997), pp. 1117–1120.

[10] J. D. Jorgensen, J. J. Faber, J. M. Carpenter, R. K. Crawford, J. R. Haumann, R. L. Hitterman, R. Kleb, G. E. Ostrowski, F. J. Rotella, and T. G. Worlton, J. Appl. Crystallogr. **22**, 321 (1989).

[11] A. C. Larson and R. B. Von Dreele (unpublished).

[12] B. Dabrowski, K. Rogacki, J. W. Koenitzer, K. R. Poeppelmeier, and J. D. Jorgensen, Physica C **277**, 24 (1997).

[13] J. D. Jorgensen, B. W. Veal, A. P. Paulikas, L. J. Nowicki, G. W. Crabtree, H. Claus, and W. K. Kwok, Phys. Rev. B **41**, 1863 (1990).

[14] J. D. Jorgensen, D. G. Hinks, O. Chmaissem, D. N. Argyriou, J. F. Mitchell, and B. Dabrowski, in *Proceedings of the 1st Polish-US Conference on High Temperature Superconductivity*, Wroclaw and Duszniki Zdrój, Poland, 1995, Lecture Notes in Physics Vol. 475, edited by J. Klamut *et al.* (Springer-Verlag, Berlin, 1996), pp. 1–15.

[15] D.-X. Chen, A. Sanchez, T. Puig, L. M. Martinez, and J. S. Munoz, Physica C **168**, 652 (1990).

[16] A. Wisniewski, R. M. Schalk, H. W. Weber, M. Reissner, W. Steiner, and J. Gorecka, Physica C **185–189**, 2211 (1991).

[17] U. Welp, G. W. Crabtree, J. L. Wagner, D. G. Hinks, P. G. Radaelli, J. D. Jorgensen, and J. F. Mitchell, Appl. Phys. Lett. **63**, 693 (1993).

[18] K. Kishio, in *Coherence in Superconductors*, edited by G. Deutscher and A. Revcolevschi (World Scientific, Singapore, 1996), pp. 212–225.

[19] O. Chmaissem, D. N. Argyriou, D. G. Hinks, J. D. Jorgensen, B. G. Storey, H. Zhang, L. D. Marks, Y. Y. Wang, V. P. Dravid, and B. Dabrowski, Phys. Rev. B **52**, 15 636 (1995).